Structural, optical and multiferroic properties of (Nd, Zn) co-doped $BiFeO_3$ nanoparticles

Huazhong Shu[1, 2, 3] • Yuhui Ma[2] • Zhongcao Wang[2] • Weiwei Mao[2, 3] • Liang Chu[3] • Jianping Yang[3] • Qiang Wu[4] •Yonggang Min[2] • Rongfang Song[1*] • Xing'ao Li[2,3**]

[1] School of Telecommunication and Information Engineering, Nanjing University of Posts and Telecommunications (NUPT), Nanjing 210023, P R China.

[2] Key Laboratory for Organic Electronics & Information Displays (KLOEID), Institute of Advanced Materials (IAM), School of Materials Science and Engineering (SMSE), Nanjing University of Posts and Telecommunications (NUPT), Nanjing 210023, PR China.

[3] Advanced Energy Technology Center & School of Science, Nanjing University of Posts and Telecommunications (NUPT), Nanjing 210023, P R China.

[4] Department of Mathematics, Physics and Electrical Engineering, University of Northumbria, Newcastle NE1 8ST United Kingdom

*Corresponding author: Rongfang Song; Tel: +86-02583492441; E-mail: songrf@njupt.edu.cn

**Corresponding author: Xing'ao Li; Tel: +86-02585866362; E-mail: lxahbmy@126.com

Abstract: The pure $BiFeO_3$(BFO) and (Nd, Zn) co-doped BFO nanoparticles were prepared by a sol-gel method. The crystal structure, optical and multiferroic properties of the samples were systematically investigated. Rietveld refinement showed that the samples crystallized in rhombhohedral R3c structure. In UV-Visible diffuse absorption spectra, an apparent blue shift can be observed after co-doping, which indicates a possible application in photocatalyst and photoconductive devices. Compared with pure BFO sample, the leakage current density of the x = 0.05 sample decreases about three orders of magnitude. The remanent magnetization (Mr) of the x = 0.10 sample reaches 0.105 emu/g while the coercive field (Hc) is as high as 7.0 kOe. The (Nd, Zn) co-doping into BFO nanoparticles has been proved to be an effective way to improve the optical and multiferroic properties.

Keywords: $BiFeO_3$; Optical properties; Ferroelectric properties; Magnetic properties; Sol-gel method

1 Introduction

Multiferroics exhibiting ferromagnetic and ferroelectric orderings in same phase have recently attracted much attention due to the fascinating fundamental physics and potential applications in spintronics,

multiple-state memories and magnetoelectric sensor devices [1-3]. Among all the multiferroic materials studied so far, lead-free BFO is the only known material showing good ferromagnetism at room temperature. BFO has been regarded as an excellent candidate for novel magnetoelectric devices for several years due to its high ferroelectric Curie temperature (T_C) of 1123 K and antiferromagnetic Neel temperature (T_N) of 647 K [1]. The G-type antiferromagnetic and ferroelectric properties of BFO are induced by rhombohedrally distorted perovskite structure with space group R3c [4]. Although the R3c symmetry permits the existence of a weak ferromagnetic moment [5], it can't be observed any net magnetization for the cause of the Dzyaloshinsky-Moriya interaction (DM interaction) [6], a cycloid type spatial spin, superimposed to the G-type antiferromagnetic spin ordering. Another drawback is the large leakage current density of BFO which prevents the practical application of BFO in the fabrication of the ferroelectric devices [7, 8]. Thus in order to improve ferromagnetic property, considerable efforts should be carried out to suppress the spiral spin structure or increase the canting level of the antiparallel spins [9]. Meanwhile it is essential to investigate how to reduce the leakage current density. It is known that the existence of leakage current density of BFO is due to the chemical valence fluctuation of Fe ions (Fe^{3+}/Fe^{2+}), oxygen vacancies, and the loss of bismuth [10]. It is widely accepted that intrinsic polarization and magnetization is associated with the lone pair of Bi^{3+} ion at the A-site and the partially-filled 3d orbitals of Fe^{3+} ion at the B-site, respectively [11]. Intrinsic BFO is an insulator with a wide bandgap of 2.5 eV, as reported by Yu et al. [12]. The photo response of BFO nanoparticles can be extended in the ultraviolet and visible region due to the fact that the microstructure, chemical structure and defects can be improved by co-doping of rare earth metal ions and transitions metal ions [13]. Therefore there is an increased possibility of utilizing the ultraviolet and visible light for photocatalysis. Some researchers have reported that nanotechnology and metal ion doping could have a great impact on their optical, electrical and magnetic properties in the last few years. Among of them, some papers focused on A-site substituting with rare earth metal ions such as Ho [14], Sm [15], Gd [16] and Ni [17], B-site substituting with transitions metal ions such as Zr [18], Co [19], Mn [20] and Zn [21], A-site and B-site substituting with (La, Pr) [22], (Sm, Cr) [23], (Gd, Ti) [24] and (Er, Ti) [25]. Physical properties of BFO can be controlled by doping, based on the fact that doping can cause the lattice distortion, control the vaporization of Bi ions and bring about the non-centrosymmetry. Furthermore, substitution at A-site with difference ionic radii can make the locked magnetization released by suppressing the spiral spin modulation of G-type antiferromagnetism [5]. The substitution

of rare earth metal ions and transitions metal ions could effectively decrease the Fe-O-Fe angle to enhance superexchange interaction between the two Fe ions to improve the magnetic properties [26-28].

In this work, polycrystalline BFO and $Bi_{1-x}Nd_xFe_{0.975}Zn_{0.025}O_3$ (x = 0.025, 0.05, 0.075 and 0.10) samples were prepared by a sol-gel method. The strategy of (Nd, Zn) co-doping was adopted to enhance optical and multiferroic properties in BFO nanopartcles. Due to the small ion size of Nd^{3+}, the crystal structure was distorted and the non-centrosymmetry of the structure was increased, which offered more space for Fe^{3+} at B-site and enhanced the electric property of the samples. The effect of (Nd, Zn) co-doped BFO nanoparticles on the crystal structure, the optical and multiferroic properties were investigated systematically and the results were discussed in detail.

2 Experimental details

The nanoparticles of pure BFO and $Bi_{1-x}Nd_xFe_{0.975}Zn_{0.025}O_3$ (x = 0.025, 0.05, 0.075 and 0.10) were prepared by a sol-gel method. The proper stoichiometric proportions of Bi_2O_3, Nd_2O_3, ZnO and $Fe(NO_3)_3 \cdot 9H_2O$ were used as starting materials and were dissolved in dilute nitric acid (analytical pure). Tartaric acid, the same amount of the total metallic ions in the precursor solution, was added into the solution as chelating agents. The solution was stirred for 7 hours in 70 ºC to form a homogeneous gel. The gel was ground into powders after drying at 80 ºC for 24 h. Then the powders were preheated at 250 ºC for 2 h and calcined at 550 ºC for 2 h.

The structure and phase purity of the samples were characterized by X-ray diffraction (XRD) (Bruker D8 Advance X-ray diffractometer) with Cu-Kα radiation at room temperature and analyzed with Rietveld refinement program. The microstructure and morphology were examined by means of scanning electron microscopy (SEM, JEOL-6380LV, Japan). Violet-visible spectrum measurements were carried out with a PerkinElmer Lambda 35 ultra violet-visible (UV/VIS) spectrophotometer. The leakage current density-electric field (J-E) curves were measured using Radiant precision materials analyzer. The magnetization hysteresis (M-H) loops of all samples were measured at room temperature using a vibrating sample magnetometer (VSM).

3 Results and discussion

X-ray diffraction (XRD) patterns of the synthesized BFO and $Bi_{1-x}Nd_xFe_{0.975}Zn_{0.025}O_3$ (x = 0.025, 0.05, 0.075 and 0.10) samples are shown in Fig. 1(a) and (b). All the diffraction peaks of pure BFO can be indexed using a rhombohedral structure, which match well with the standard reported values (JCPDS File No. 71-2494). Fig. 1(b) shows the enlarged view of the diffraction peaks (1 0 4) and (1 1 0) in the vicinity of $2\theta = 32^{\circ}$. The (1 0 4) peak shifts towards high diffraction angle gradually with increasing Nd concentration, while the (1 10) peak remains almost unchanged. In order to reveal more about phase changes and lattice parameters, Rietveld refinements using Fullprof suite have been performed. Fig. 2 shows the Rietveld refinement results of the pure BFO and (Nd, Zn) co-doped samples. The refinements were carried out using space group, lattice constants and Fe-O-Fe bond angle to find best fit between observed and calculated patterns. Selected structural parameters and R- factors are listed in Table 1. Rietveld refinement shows that all samples well fit with rhombohedral structure with space group R3c. Relatively small R factors of all the samples were obtained, which indicated that the conclusion is reliable and effective. The Bi-O bond and Fe-O bond distance of all samples have the same trend of change. It can be seen from Table 1 that the two Bi-O bond and Fe-O bond distance have opposite behaviors. They don't change much up to x=0.05 and then start to depart (one increasing and the other decreasing) for x>0.05. The Fe-O-Fe bond angle decreases as (Nd, Zn) co-doped concentration increase. All of these cause the asymmetry strengthened. The variations of structural parameters may be caused by the ionic radius of (Nd, Zn) co-dopants due to the difference of ionic radius (rZn^{2+} = 0.75 Å > rFe^{3+} = 0.645 Å and rNd^{3+} = 0.983 Å < rBi^{3+} = 1.03 Å). The results of the XRD and Rietveld refinement revealed that the (Nd, Zn) co-doping caused internal structure distortion related to changes in Fe-O bond distances and bond angles [29]. According to the above results, it is observed that (Nd, Zn) ions are effectively incorporated into the crystal structure of BFO, which may play an important role on improving optical and multiferroic properties.

SEM images of pure BFO and $Bi_{1-x}Nd_xFe_{0.975}Zn_{0.025}O_3$ (x = 0.025, 0.05, 0.075 and 0.10) samples are shown in Fig. 3. The crystal grains of pure BFO are non-uniform and irregular in shape with the average grain size about 200 nm. It can be seen that the average grain sizes of all samples have trend drab and smaller with the increasing Nd concentration. The x = 0.025 sample has a certain degree of agglomeration with the average grain size about 150 nm and the average grain

sizes of samples with x = 0.05, 0.075 and 0.10 are about 120 nm, 80 nm and 60 nm respectively, as shown in Fig. 3 (a), (b) , (c), (d) and (e). The average grain sizes decrease from 200 to 60 nm after (Nd, Zn) co-doping, suggesting that (Nd, Zn) content of BFO inhibits the grain growth, which can be used to control the growth of grain size. In general, it is believed that the smaller the grain sizes, the more the defects at the grain boundaries, which may have significant influence on the optical and multiferroic properties of the nanoparticles [30, 31].

Many researchers recognized BFO was a fascinating optical material, which could be applied in photocatalyst and photoconductive devices [32]. It is well known that the optical transmittance properties are relevant to the electronic structure features and band gaps. Fig. 4 shows UV-Visible diffuse absorption spectra of pure BFO and $Bi_{1-x}Nd_xFe_{0.975}Zn_{0.025}O_3$ (x = 0.025, 0.05, 0.075 and 0.10) samples in the wavelength range 300 - 900 nm. Pristine BFO nanoparticles exhibit an absorption peak around 550 nm. Compared with pure BFO, an apparent blue shift can be observed in the co-doped samples. As shown in Fig. 4, the photo response of the co-doped BFO nanoparticles has been extended in the ultraviolet and visible region, which can be used to detect ultraviolet and visible light in the photocatalysis [33]. Optical band gaps (Eg) of pure BFO and $Bi_{1-x}Nd_xFe_{0.975}Zn_{0.025}O_3$ (x = 0.025, 0.05, 0.075 and 0.10) samples can be calculated using classical Tauc formula. Based on the theory of optical absorption, the absorption coefficient (α) and the photon energy (hν) for direct allowed transitions are related as: $(\alpha h\nu)^2 = A(h\nu - Eg)$, where A is a constant function. Fig. 5 shows the $(\alpha h\nu)^2$ vs hν plots. By extrapolating straight line, each Eg value of all the samples is 1.55ev, 1.74ev, 1.79ev and 1.70ev, with the corresponding (Nd, Zn) co-doped concentration x=0.025, 0.05, 0.075 and 0.10, respectively. The band gap values were observed to increase with the concentration and then decrease, having a maximum in the x=0.05-0.075 region, which may be caused by the change of Fe-O-Fe bond angle and Bi-O bond and Fe-O bond distance.

The leakage current mechanisms for pure BFO and $Bi_{1-x}Nd_xFe_{0.975}Zn_{0.025}O_3$ (x = 0.025, 0.05, 0.075 and 0.10) samples at room temperature were displayed by the plots of log (J) versus E as shown in Fig. 6. It can be seen that each J-E curve of the samples is symmetry around the current density axis. The leakage current density decreases with the concentration x = 0.025 and x = 0.05. However, the leakage current density does not reduces when the concentration x increases from 0.075 to 0.10, which can be interpreted by the change of Bi-O bond and Fe-O bond

distance. Compared with pure BFO sample, the leakage current density of the x = 0.05 sample decreases about three orders of magnitude at all applied electric field. As known, the high leakage current in BFO system is caused mainly by charge defects such as bismuth vacancies, oxygen vacancies and Fe^{+2} contents [7, 34, 35]. This indicates that the leakage current property can be improved effectively by co-doping proper concentration of (Nd, Zn) into BFO based on the fact that the (Nd, Zn) co-doped samples can reform the structural and enhance superexchange interactions of Fe^{2+} and Fe^{3+}.

Fig. 7 shows the magnetization versus magnetic field (M-H) curves of pure BFO and $Bi_{1-x}Nd_xFe_{0.975}Zn_{0.025}O_3$ (x = 0.025, 0.05, 0.075 and 0.10) samples with a maximum applied magnetic field of ±30 kOe at room temperature. The magnetization of pure BFO increases linearly with magnetic field (H) up to 30 kOe, for the case that pure BFO shows a weak ferromagnetic order due to the anitiferromagnetic spin structure. As shown, the (Nd, Zn) co-doped samples exhibit larger magnetization at room temperature than that of the pure BFO sample. The remanent magnetization (Mr) of the x = 0.10 sample reaches 0.105 emu/g while the coercive field (Hc) is as high as 7.0 kOe. This can be interpreted that the Fe-O bond angle decreases from 158.45º to: 154.9117º, 150.9º, 144º and 142º, with the increasing Nd concentration (x = 0.025, 0.05, 0.075 and 0.10), as seen in Table. 1. The Fe-O bond distance and bond angle play an important role on the structure transformation [29], which release the suppression of the spin cycloid and enhance G-type antiferromagnetic and ferroelectric properties of BFO.

4 Conclusions

In this paper, BFO and (Nd, Zn) co-doped BFO samples were prepared by a sol-gel method. The co-doped BFO samples still maintained the rhombohedral (R3c) as pure BFO which were all analyzed by XRD and Rietveld refinement. The size and morphology of the nanoparticles had been displayed using SEM. The optical property was also investigated on the UV-visible absorption spectra and optical band gap. The co-doped samples showed lower current leakage density and higher ferromagnetic properties with proper Nd concentration. This work provides an alternative strategy to enhance multiferroic properties, which is a useful try for the practical applications in the future.

Acknowledgements

We acknowledge the financial support from the Ministry of Education of China (No. IRT1148), Jiangsu Synergistic Innovation Center for Advanced Materials (SICAM), the Project Funded by the Priority Academic Program Development of Jiangsu Higher Education Institutions (PAPD, YX03001), the National Natural Science Foundation of China (51372119, 61377019, 61136003, 51173081), College Postgraduate Research and Innovation Project of Jiangsu Province (KYLX_0794, KYLX15_0848), the Natural Science Foundation of Jiangsu (BX20150860) and the Natural Science Foundation of NJUPT (NY214129, NY214130, NY214181,NY215022).

References

1. Wang, J., Neaton, J.B., Zheng, H., Nagarajan, V., Ogale, S.B., Liu, B., Viehland, D., Vaithyanathan, V., Schlom, D.G., Waghmare, U.V., Spaldin, N.A., Rabe, K.M., Wuttig, M., Ramesh, R.: Epitaxial $BiFeO_3$ multiferroic thin film heterostructures. Science **299**(5613), 1719-1722 (2003).
2. Eerenstein, W., Mathur, N.D., Scott, J.F.: Multiferroic and magnetoelectric materials. Nature **442**(7104), 759-765 (2006).
3. Cheong, S.W., Mostovoy, M.: Multiferroics: a magnetic twist for ferroelectricity. Nature Materials **6**, 13-20 (2007).
4. Ravindran, P., Vidya, R., Kjekshus, A., Fjellvåg, H., Eriksson, O.: Theoretical investigation of magnetoelectric behavior in$BiFeO_3$. Phys Rev B **74**(22) (2006).
5. Ederer, C., Spaldin, N.A.: Weak ferromagnetism and magnetoelectric coupling in bismuth ferrite. Phys Rev B **71**(6) (2005).
6. Kumar, P., Kar, M.: Effect of structural transition on magnetic and dielectric properties of La and Mn co-substituted $BiFeO_3$ ceramics. Mater Chem Phys **148**, 968-977 (2014).
7. Qi, X., Dho, J., Tomov, R., Blamire, M.G., MacManus-Driscoll, J.L.: Greatly reduced leakage current and conduction mechanism in aliovalent-ion-doped $BiFeO_3$. Appl Phys Lett **86**(6), 062903 (2005).
8. Pradhan, S.K., Das, J., Rout, P.P., Mohanta, V.R., Das, S.K., Samantray, S., Sahu, D.R., Huang, J.L., Verma, S., Roul, B.K.: Effect of holmium substitution for the improvement of multiferroic properties of $BiFeO_3$. J Phys Chem Solids **71**(11), 1557-1564 (2010).
9. Mao, W., Wang, X., Han, Y., Li, X.a., Li, Y., Wang, Y., Ma, Y., Feng, X., Yang, T., Yang, J., Huang, W.: Effect of Ln (Ln=La, Pr) and Co co-doped on the magnetic and ferroelectric properties of $BiFeO_3$ nanoparticles. J Alloy Compd **584**, 520-523 (2014).
10. Godara, S., Sinha, N., Kumar, B.: Study the influence of Nd and Co/Cr co-substitutions on structural, electrical and magnetic properties of $BiFeO_3$ nanoparticles. Ceram Int **42**(1), 1782-1790 (2016).
11. Ederer, C., Spaldin, N.A.: Recent progress in first-principles studies of magnetoelectric multiferroics. Curr Opin Solid St M **9**(3), 128-139 (2005).

12. Yu, X., An, X.: Enhanced magnetic and optical properties of pure and (Mn, Sr) doped $BiFeO_3$ nanocrystals. Solid State Commun **149**(17-18), 711-714 (2009).
13. Han, Y., Ma, Y., Quan, C., Gao, N., Zhang, Q., Mao, W., Zhang, J., Yang, J., Li, X.a., Huang, W.: Substitution-driven structural, optical and magnetic transformation of Mn, Zn doped $BiFeO_3$. Ceram Int **41**(2), 2476-2483 (2015).
14. Suresh, P., Babu, P.D., Srinath, S.: Effect of Ho substitution on structure and magnetic properties of $BiFeO_3$. J Appl Phys **115**(17), 17D905 (2014).
15. Kumar, A., Yadav, K.L.: A systematic study on magnetic, dielectric and magnetocapacitance properties of Ni doped bismuth ferrite. J Phys Chem Solids **72**(11), 1189-1194 (2011).
16. Pattanayak, S., Parida, B.N., Das, P.R., Choudhary, R.N.P.: Impedance spectroscopy of Gd-doped $BiFeO_3$ multiferroics. Appl Phys A **112**(2), 387-395 (2012).
17. Zhao, J., Zhang, X., Liu, S., Zhang, W., Liu, Z.: Effect of Ni substitution on the crystal structure and magnetic properties of $BiFeO_3$. J Alloy Compd **557**, 120-123 (2013).
18. Arora, M., Chauhan, S., Sati, P.C., Kumar, M.: Effect of Non-magnetic Ions Substitution on Structural, Magnetic and Optical Properties of $BiFeO_3$ Nanoparticles. J Supercond Nov Magn **27**(8), 1867-1871 (2014).
19. Ray, J., Biswal, A.K., Acharya, S., Ganesan, V., Pradhan, D.K., Vishwakarma, P.N.: Effect of Co substitution on the magnetic properties of $BiFeO_3$. J Magn Magn Mater **324**(23), 4084-4089 (2012).
20. Hunpratub, S., Thongbai, P., Yamwong, T., Yimnirun, R., Maensiri, S.: Effects of Mn Doping on the Dielectric Relaxations and Dielectric Response in Multiferroic $BiFeO_3$ Ceramics. J Supercond Nov Magn **25**(5), 1619-1622 (2012).
21. Chaudhari, Y.A., Singh, A., Abuassaj, E.M., Chatterjee, R., Bendre, S.T.: Multiferroic properties in $BiFe_{1-x}Zn_xO_3$ (x=0.1-0.2) ceramics by solution combustion method (SCM). J Alloy Compd **518**, 51-57 (2012).
22. Sharma, P., Verma, V.: Structural, magnetic and electrical properties of La and Mn co-substituted BFO samples prepared by the sol-gel technique. J Magn Magn Mater **374**, 18-21 (2015).
23. Liu, W., Tan, G., Dong, G., Ren, H.: Lattice distortion and room-temperature ferroelectric properties of (Sm, Cr) co-doped $BiFeO_3$ thin films. J Mater Sci-mater El **24**(11), 4296-4301 (2013).
24. Kumar, M., Sati, P.C., Chhoker, S.: Electron spin resonance study and improved magnetic and dielectric properties of Gd–Ti co-substituted $BiFeO_3$ ceramics. J Mater Sci-mater El **25**(12), 5366-5374 (2014).
25. Ma, Y., Xing, W., Chen, J., Bai, Y., Zhao, S., Zhang, H.: The influence of Er, Ti co-doping on the multiferroic properties of $BiFeO_3$ thin films. Appl Phys A **122**(2) (2016).
26. Paudel, T.R., Jaswal, S.S., Tsymbal, E.Y.: Intrinsic defects in multiferroic $BiFeO_3$and their effect on magnetism. Phys Rev B **85**(10) (2012).
27. Suresh, P., Babu, P.D., Srinath, S.: Effect of Ho substitution on structure and magnetic properties of $BiFeO_3$. J Appl Phys **115**(17), 17D905 (2014).
28. Wen, X., Chen, Z., Liu, E., Lin, X., Chen, C.: Effect of Ba and Mn doping on microstructure and multiferroic properties of $BiFeO_3$ ceramics. J Alloy Compd **678**, 511-517 (2016).
29. Modak, P., Lahiri, D., Sharma, S.M.: Correlation between Structure and Ferromagnetism in Nano-$BiFeO_3$. J Phys Chem C **120**(15), 8411-8416 (2016).
30. Dhanalakshmi, R., Muneeswaran, M., Vanga, P.R., Ashok, M., Giridharan, N.V.: Enhanced photocatalytic activity of hydrothermally grown $BiFeO_3$ nanostructures and role of catalyst recyclability in photocatalysis based on magnetic framework. Appl Phys A **122**(1) (2015).

31. Gupta, S., Tomar, M., Gupta, V.: Ferroelectric photovoltaic properties of Ce and Mn codoped $BiFeO_3$ thin film. J Appl Phys **115**(1), 014102 (2014).
32. Kumar, P., Kar, M.: Effect of structural transition on magnetic and optical properties of Ca and Ti co-substituted $BiFeO_3$ ceramics. J Alloy Compd **584**, 566-572 (2014).
33. Wang, S., Chen, D., Niu, F., Zhang, N., Qin, L., Huang, Y.: Enhancement in visible light photocatalytic activity of $BiFeO_3$ photocatalysts by Pd cocatalyst. Appl Phys A **122**(9), 867 (2016).
34. Vijayasundaram, S.V., Suresh, G., Mondal, R.A., Kanagadurai, R.: Substitution-driven enhanced magnetic and ferroelectric properties of $BiFeO_3$ nanoparticles. J Alloy Compd **658**, 726-731 (2016).
35. Mao, W., Chen, W., Wang, X., Zhu, Y., Ma, Y., Xue, H., Chu, L., Yang, J., Li, X.a., Huang, W.: Influence of Eu and Sr co-substitution on multiferroic properties of $BiFeO_3$. Ceram Int **42**(11), 12838-12842 (2016).

Figure captions

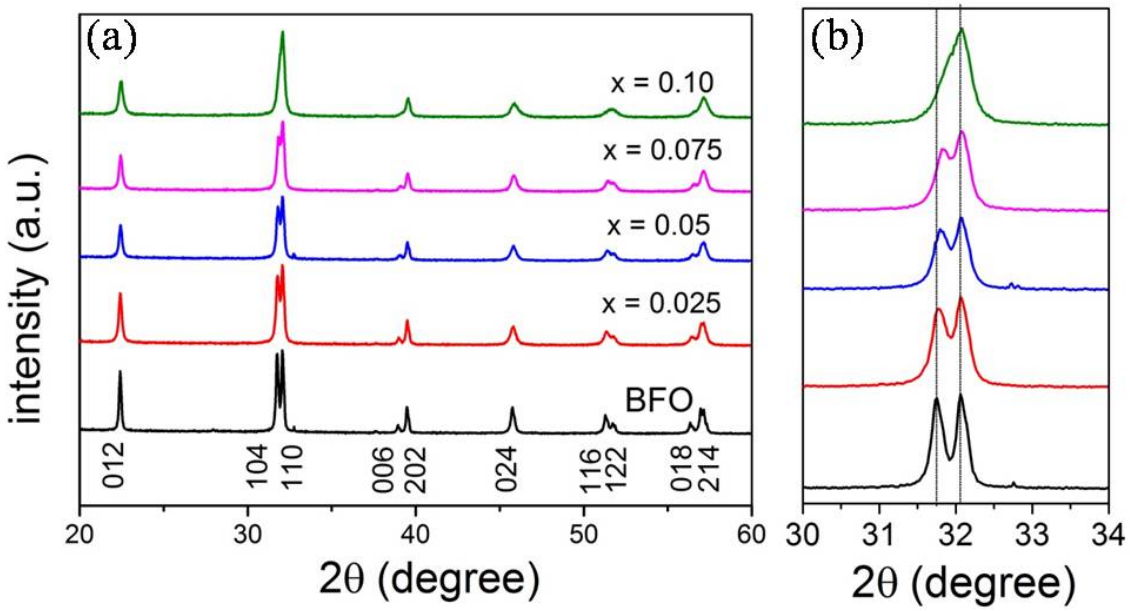

Fig. 1.**(a)** XRD patterns of pure BFO and $Bi_{1-x}Nd_xFe_{0.975}Zn_{0.025}O_3$ (x = 0.025, 0.05, 0.075 and 0.10) samples. **(b)** Enlarged view of the diffraction peaks (104) and (110) in the vicinity of 2θ = 32 º.

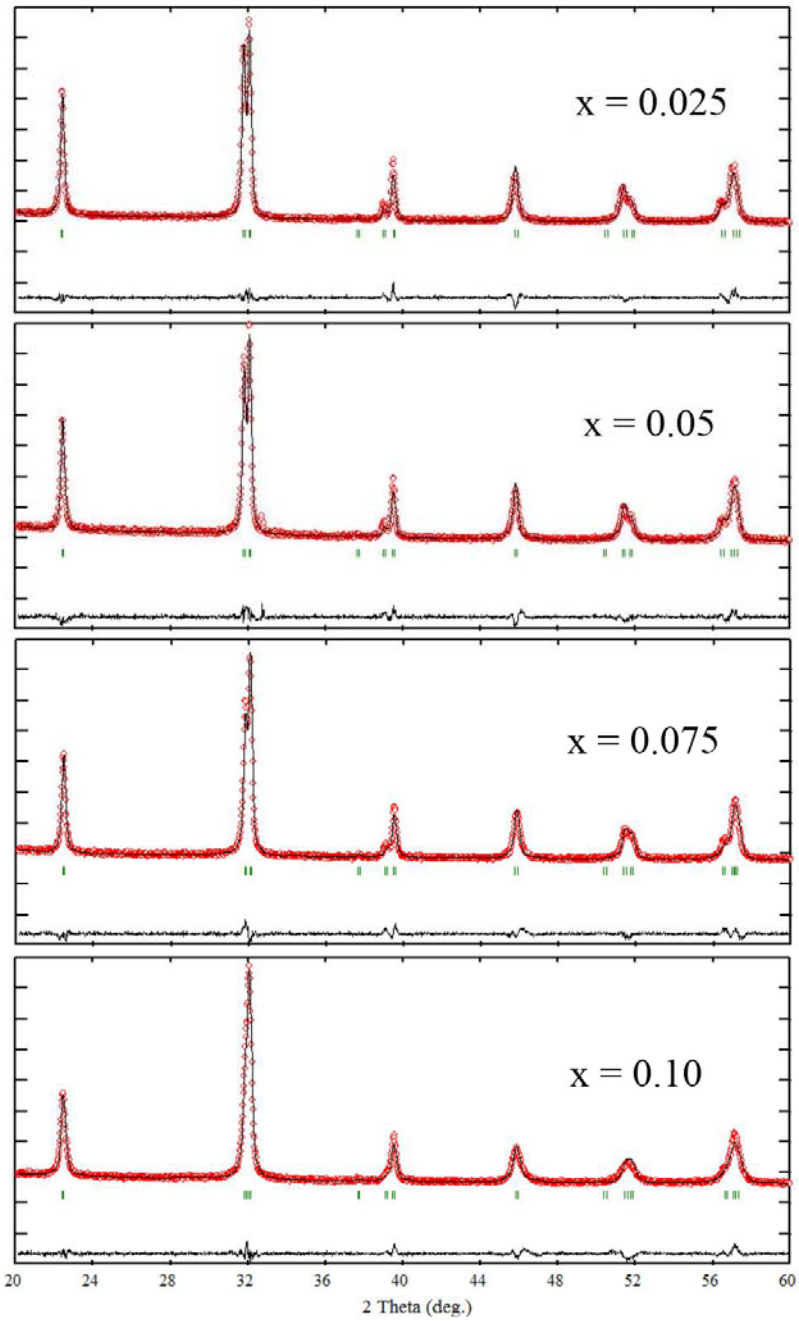

Fig. 2. XRD Rietveld refinement results for $Bi_{1-x}Nd_xFe_{0.975}Zn_{0.025}O_3$ (x = 0.025, 0.05, 0.075 and 0.10) samples. (a) x = 0.025, (b) x = 0.05, (c) x = 0.075 and (d) x = 0.10, respectively. Observed (red) and calculated (black).

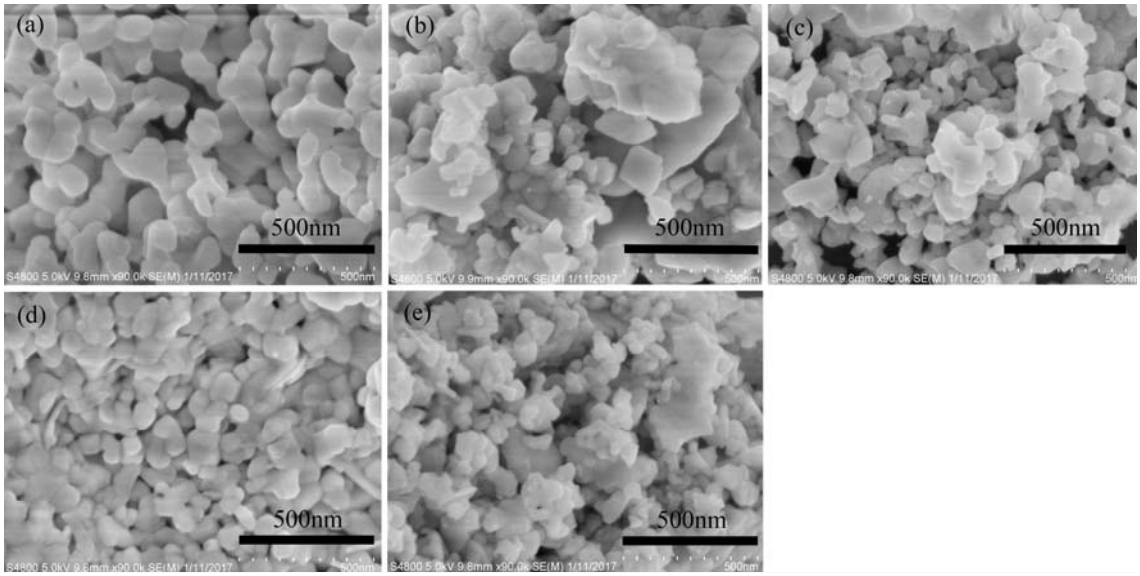

Fig. 3. SEM images of pure BFO and $Bi_{1-x}Nd_xFe_{0.975}Zn_{0.025}O_3$ (x = 0.025, 0.05, 0.075 and 0.10) samples. (a) BFO, (b) x = 0.025, (c) x = 0.05, (d) x = 0.075 and (e) x = 0.10 respectively.

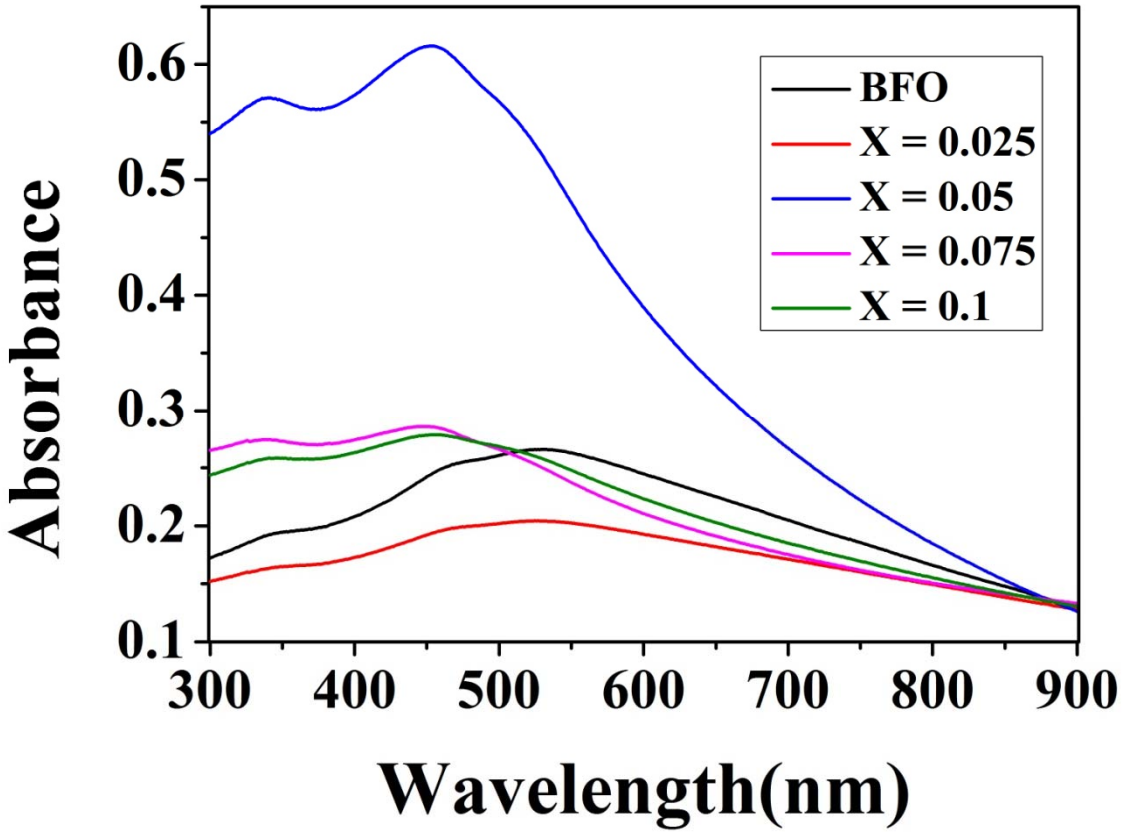

Fig. 4. UV–visible absorption spectra of BFO and (Nd, Zn) co-doping samples.

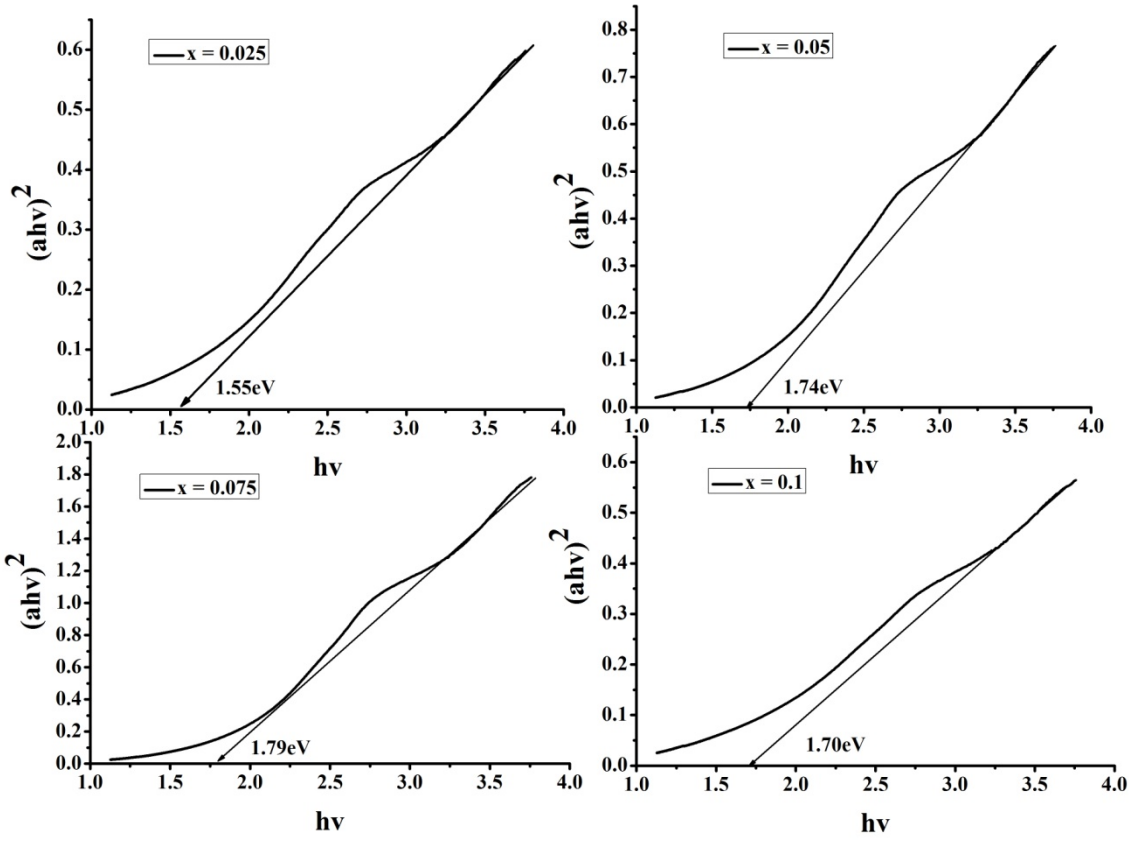

Fig. 5. Tauc's plots to determine the band gap of (Nd, Zn) co-doping samples respectively.

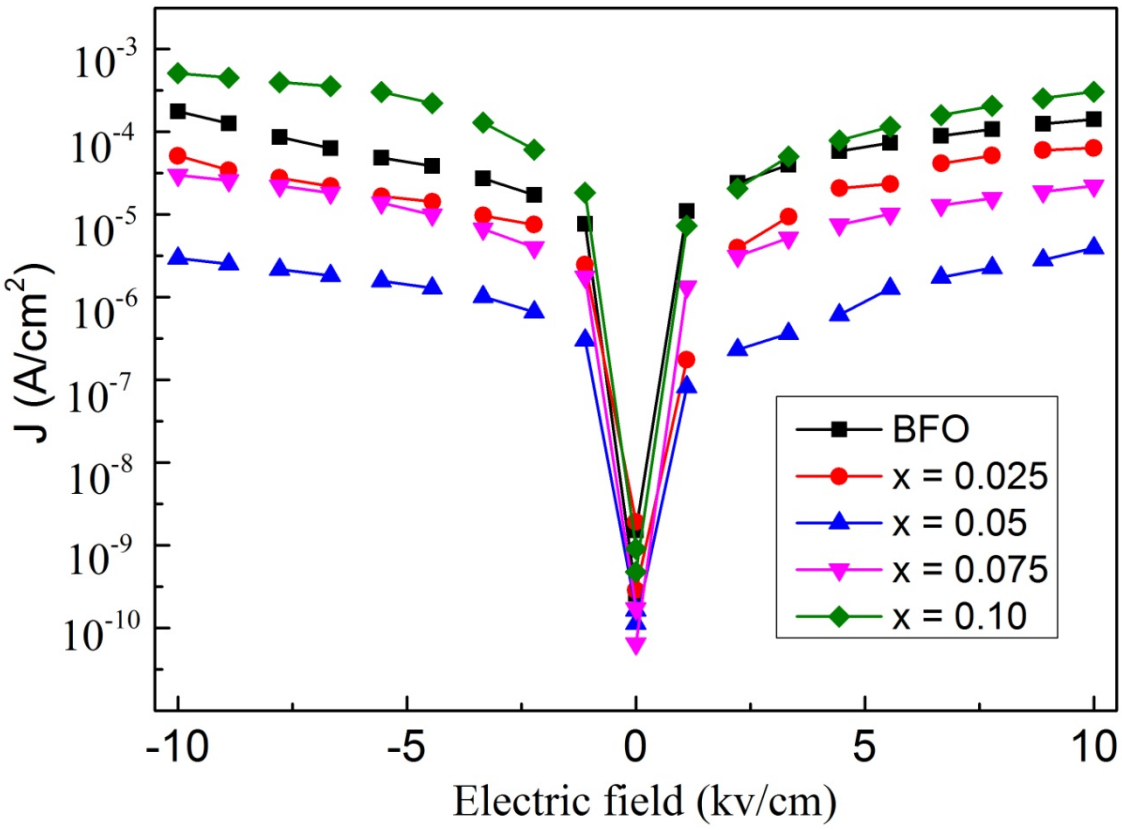

Fig.6. Leakage current density of pure BFO and $Bi_{1-x}Nd_xFe_{0.975}Zn_{0.025}O_3$ (x = 0.025, 0.05, 0.075 and 0.10) samples at room temperature.

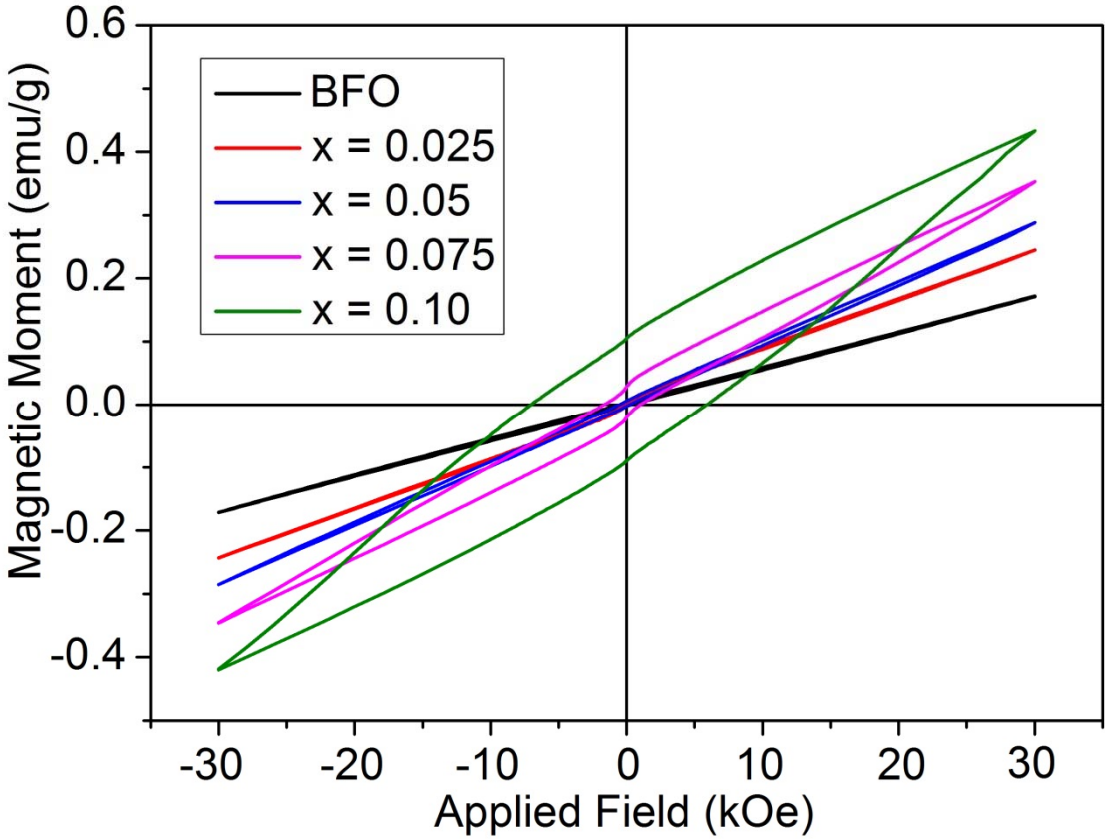

Fig. 7. The magnetization versus magnetic field (M-H) curves of pure BFO and $Bi_{1-x}Nd_xFe_{0.975}Zn_{0.025}O_3$ (x = 0.025, 0.05, 0.075 and 0.10) samples at Room temperature

Table 1 Selected structural parameters from Rietveld refinement of pure BFO and $Bi_{1-x}Nd_xFe_{0.975}Zn_{0.025}O_3$ (x = 0.025, 0.05, 0.075 and 0.10) samples.

Sample	Cell Type	Cell(Å)	Bi-O bond distance(Å)	Fe-O bond distance(Å)	Fe-O-Fe,°	R factors	Bragg R-factor	Rf-factor
BFO	**R3c**	**a=5.5806 b=5.5806 c=13.8748 V=374.2159**	**2.5903 /2.3049**	**1.8773 /2.1595**	**158.45**	**Rp=16.1 Rwp=13.0 Re=10.2 GOF=1.3**	**1.59**	**1.8**
X=0.025	**R3c**	**a=5.5601 b=5.5601 c=13.8090 V=369.7126**	**2.5072 /2.3588**	**1.9356 /2.1108**	**154.9117**	**Rp=15.2 Rwp=13.1 Re=9.70 GOF=1.3**	**1.79**	**1.88**
X=0.05	**R3c**	**a=5.5813 b=5.5813 c=13.8492 V=373.6109**	**2.5232 /2.2655**	**1.8534 /2.2404**	**150.9**	**Rp=15.5 Rwp=13.1 Re=10.5 GOF=1.2**	**1.92**	**1.91**
X=0.075	**R3c**	**a=5.5856 b=5.5856 c=13.8442 V=374.0578**	**2.9236 /1.8540**	**1.8415 /2.3475**	**144**	**Rp=16.1 Rwp=13.3 Re=10.6 GOF=1.2**	**1.66**	**1.77**
X=0.01	**R3c**	**a=5.5800 b=5.5800 c=13.8095 V=372.3739**	**2.9685 /1.7228**	**1.7097 /2.4480**	**142**	**Rp=16.3 Rwp=13.9 Re=10.3 GOF=1.3**	**1.48**	**1.66**